Available online at www.sciencedirect.com
SCIENCE DIRECT®
PERGAMON
Computers and Structures 81 (2003) 2301–2317
Computers & Structures
www.elsevier.com/locate/compstruc

Modelling of SMA materials: Training and two way memory effects

F. Auricchio [a], S. Marfia [b,*], E. Sacco [b]

[a] Department of Structural Mechanics, University of Pavia, Via Ferrata 1, 27100 Pavia, Italy
[b] Department of Mechanics, Structures and Environment, University of Cassino, Via G. Di Biasio, 43, 03043 Cassino, Italy

Received 25 November 2002; accepted 3 July 2003

Abstract

The present work addresses a simple and effective one-dimensional model able to reproduce the superelastic behaviour as well as the shape memory effect. In particular, it considers the transformations from austenite to single variant martensite and from single variant martensite to austenite, taking into account the influence of the temperature. Moreover, the training and the two way memory effects are modelled considering the evolutions of the phase-transformation stress thresholds as well as of the residual "permanent" deformation. The time integration of the evolutive equations is performed adopting a backward Euler scheme and the finite time step is solved through a modified return-map algorithm. The proposed SMA constitutive law and numerical procedure are adopted to develop numerical applications. Finally, the ability of the model to reproduce experimental data is assessed.

Keywords: Shape-memory alloys; Pseudoelastic behaviour; Shape memory effects; Training effects; Two way memory effects; Numerical procedure

1. Introduction

Shape-memory alloys (SMA) belong to a family of materials, which are able to recover large deformations. In fact, for temperature greater or lower than a certain value, they present the so-called pseudoelastic (superelastic) behaviour or the shape memory effect, i.e. they can recover large deformations during the unloading or through a suitable thermal cycle. The very special behaviour of the shape-memory alloys is due to their capability to undergo reversible changes of the crystallographic structure, depending on the temperature and on the stress state [12,14,23]. These changes can be interpreted as martensitic transformations between a crystallographic more-ordered parent phase, the austenite (A), and a crystallographic less-ordered product phase, the martensite (M) [29]. In general, the austenite is stable at high values of temperature and low values of stresses, while the martensite is stable at low values of temperature and high values of stresses.

Due to the pseudoelasticity and shape memory effects, shape-memory alloys are successfully adopted in a broad set of advanced and innovative applications in aeronautical, biomedical, mechanical and civil engineering [3,5,6,13,14]. The high interest toward the use of SMA in commercially valuable applications clearly requires the use of accurate constitutive models during the design phase of devices.

Several models able to reproduce the SMA constitutive behaviour were proposed in literature. A recent state of the art regarding the behaviour, the modelling and the applications of SMA can be found in the book [9], where wide reference lists on the different SMA aspects are reported. The available models can be framed into three categories: the micro-level models which

* Corresponding author. Tel.: +39-0776-299745; fax: +39-0776-299392.
E-mail address: marfia@unicas.it (S. Marfia).

0045-7949/$ - see front matter © 2003 Elsevier Ltd. All rights reserved.
doi:10.1016/S0045-7949(03)00319-5

describe micro-scale level effects, such as, nucleation, interface motion, twin growth [1,15]; the micro–macro-level models which combine micro-mechanical elements, such as habit planes, martensitic variants, with macro-scale thermodynamics and adopt proper homogenization techniques to derive macro/global parameters from the micro/local ones [11,19,17,26]; the macro-level models which are able to describe some of the major SMA macroscopic features [18,4,24,27,7,25,8]. The macro-models are particularly suitable for the study of SMA structural elements as they can be implemented more easily in numerical codes.

One of the most interesting feature is the SMA response under cyclic loading conditions. In fact the material response progressively changes during the cycles, reaching a limit and stable path after a certain number of stress/temperature loading–unloading cycles, i.e. after the so-called material training. From a phenomenological point of view the training effects on the stress–strain curve result in the two following aspects:

- a progressive decrement of the initial and final stress thresholds of the phase transformations,
- a progressive increment of a residual "permanent" deformation.

Both the described phenomena have a micro-mechanical interpretation which is still under investigation. In particular, two micromechanical interpretations are discussed in literature, one based on residual stresses due to the development of dislocations induced in the material during the cycles, the other on residual permanent martensite accumulated during training [16]. Referring to the first interpretation, the progressively change in the SMA response under cyclic loading is attributed to the oriented residual stresses occurring during the dislocations arrangement. The nucleation and growth of preferential martensite variants are favored by these residual stresses that tend to be relaxed by shape change. Moreover, since the generation of dislocations is strictly linked to the development of plasticity, it can be deduced that the training effects are connected with a residual plastic strain. The second interpretation is based on the progressive increment of residual permanent oriented martensite variants that occur because of the dislocations arrangement. The presence of the dislocations does not allow the complete martensite–austenite transformation during the unloading and heating process. Moreover, the small residual martensite plates grow during subsequent cycles.

The presence of permanent deformation, due to plastic strains or to the residual martensite variants, occurring during the material training allows to obtain reversible spontaneous shape change during cooling and heating processes without application of any external stress, which is known as the two way memory effect (TWME). This effect can be used to realize new potential applications, as reversible fasteners, temperature-sensitive actuators, retrievable medical implants, toys and novelty items.

SMA models which take into account the training effects and the two way memory effect have been presented in literature. Among the others, Tanaka et al. [28] developed a model for the cyclic uniaxial response of shape-memory alloys subjected to thermal and/or mechanical loads based on three internal variables, the local residual stress and strain and the residual volume fraction of martensite accumulated during cycles. Lexcellent and Bourbon [20] proposed a one-dimensional pseudoelastic model for the analysis of the tensile cyclic response of SMA, introducing a new internal state parameter representing the instantaneous residual martensite volume fraction. Abeyaratne and Sang-Joo Kim [2] developed a one-dimensional model based on an energetic approach, assuming that the critical value of the driving forces required for nucleating and propagating the phase transformations is affected by the defect density which depends on the number of loading cycles. Bo and Lagoudas [10] described a one-dimensional model which accounts for the training effects introducing irreversible plastic strain. Lexcellent et al. [21] developed a model in the framework of thermodynamics introducing a training term in the expression of the free energy of self-accommodated martensite.

The present work addresses a one-dimensional (1D) model able to reproduce the pseudoelastic and shape memory behaviour of SMA under cyclic loading conditions, including training and two way memory effects. The aim is to develop a one-dimensional model that is able to take into account many of the special features of SMA behaviour, such as the different response in tension and in compression, the different elastic properties of austenite and martensite, the reorientation process, the training effects and the TWME, and at the same time that is suitable for the implementation in a numerical code.

The choice to develop a one-dimensional model is motivated by the fact that most of structural elements in SMA applications can be designed using 1D constitutive relations, involving the bending and axial response of beams. Furthermore, in a 1D frame, it is possible to accurately account for the above mentioned several special features of SMA behaviour.

In the model the transformations from austenite to single variant martensite and from single variant martensite to austenite are considered, taking into account the influence of the temperature. Moreover, the micromechanical interpretation that assumes the training effects due to the residual permanent martensite fraction is adopted. Hence, the material training under cyclic loading is modeled adopting exponential evolutions of the austenite–martensite transformation stress thresh-

olds and of the residual "permanent" deformation. Constitutive equations are written in evolutive form. The time integration of the evolutive equations is performed adopting a backward Euler scheme and the finite time step is solved through a modified return-map algorithm. The proposed SMA constitutive law and numerical procedure are adopted to develop numerical applications. Finally, the ability of the model to reproduce experimental data and the TWME is assessed.

The paper is organized as follows. First a one-dimensional model is presented, then the time-discrete integration algorithm for the model, together with a solution algorithm belonging to the return map family, is described. Finally, some numerical results, which show the model ability to simulate the axial and bending behaviour of SMA under cyclic loading, are presented.

2. Time-continuous model

In the following an uniaxial model able to describe the pseudoelastic and shape memory effects of SMA under cyclic loading conditions is presented. In Fig. 1, all the possible phase transformations for the shape-memory alloys are reported.

The pseudoelastic effect occurs when a loading–unloading cycle is performed at a temperature higher then $T_{\mathrm{f}}^{\mathrm{SA}}$ while the shape memory effect is obtained by a combination of stress and temperature path.

A scalar internal variable ξ_{S}, which represents the single variant martensite fraction, is introduced.

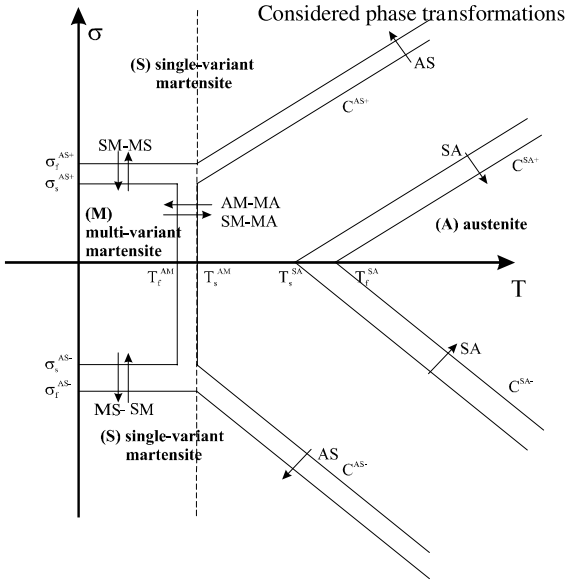

Fig. 1. Scheme of the phase transformation in uniaxial tension and compression versus temperature.

Two evolutionary processes which may produce variations of ξ_{S} are considered:

- the conversion of austenite into single variant martensite ($\mathrm{A} \to \mathrm{S}$),
- the conversion of single variant martensite into austenite ($\mathrm{S} \to \mathrm{A}$).

Hence the analysis is restricted to the case that the temperature is greater than $T_{\mathrm{s}}^{\mathrm{AM}}$, i.e. only austenite—single variant martensite phase transformations are considered. The austenite volume fraction is obtained as:

$$\xi_{\mathrm{A}} = 1 - \xi_{\mathrm{S}} \tag{1}$$

In the present model, the micromechanical interpretation that considers the progressive increment of the permanent deformation during cyclic loading due to an increment of the irreversible residual martensite fraction is adopted. Thus, the martensite fraction is set as:

$$\xi_{\mathrm{S}} = \xi_{\mathrm{R}} + \xi \tag{2}$$

where ξ represent the reversible martensite fraction and ξ_{R} is the residual irreversible martensite fraction.

2.1. Strain decomposition and elastic relation

Limiting the discussion to a small deformation regime, the additive decomposition of the total strain ε is considered:

$$\varepsilon = \varepsilon^{\mathrm{e}} + \xi_{\mathrm{S}}\beta - \xi_{\mathrm{R}}(\beta - \kappa) + \alpha(T - T_0) \tag{3}$$

where ε^{e} is the elastic strain, $\xi_{\mathrm{S}}\beta$ is the inelastic strain due to the phase transition; in particular, β is an internal variable describing the change of martensite reorientation [7,22], κ is a training parameter whose value is set in the next subsection, α is the thermal coefficient and T_0 is the reference temperature.

The elastic strain is assumed to be linearly related to the stress:

$$\sigma = E\varepsilon^{\mathrm{e}} = E(\varepsilon - \xi_{\mathrm{S}}\beta + \xi_{\mathrm{R}}(\beta - \kappa) - \alpha(T - T_0)) \tag{4}$$

where E is the elastic modulus, given by:

$$E(\xi_{\mathrm{S}}) = \frac{E_{\mathrm{A}}E_{\mathrm{S}}}{E_{\mathrm{S}} + \xi_{\mathrm{S}}(E_{\mathrm{A}} - E_{\mathrm{S}})} \tag{5}$$

with E_{A} and E_{S} the Young moduli for the austenite and single variant martensite, respectively. Eq. (5) is obtained from the homogenization theory adopting the Reuss scheme [6].

2.2. Kinetic rules

Kinetic rules in terms of the uniaxial deformation are introduced for both the phase transitions, following experimental evidences. In particular, it is set:

$$\dot{\xi}_S = \dot{\xi}_S^{AS} + \dot{\xi}_S^{SA}$$

where $\dot{\xi}_S^{AS}$ and $\dot{\xi}_S^{SA}$ represent the single variant martensite fraction volume rates occurring during the austenite–single variant martensite and single variant martensite–austenite phase transformations, respectively. It can be noted that $\dot{\xi}_S^{AS}$ and $\dot{\xi}_S^{SA}$ cannot be simultaneously different form zero.

- Transition $A \to S$

$$\dot{\xi}_S^{AS} = \pi^{AS}(1-\xi_S)\frac{\dot{G}^{AS}}{\left(S_f^{AS} - G^{AS}\right)^{\alpha^{AS}}}\mathscr{H}^{AS} \tag{6}$$

where

$$G^{AS} = \eta - \frac{C^{AS}}{E}T \tag{7}$$

$$S_f^{AS} = \frac{\sigma_f^{AS} - C^{AS}T_s^{AM}}{E_S} + R_f^{AS} \tag{8}$$

$$S_s^{AS} = \frac{\sigma_s^{AS} - C^{AS}T_s^{AM}}{E} + R_s^{AS} \tag{9}$$

with

$$\text{if } \sigma \geqslant 0 \quad \begin{cases} \eta = \varepsilon \\ R_s^{AS} = \xi_S\beta - \xi_R(\beta - \kappa) \\ R_f^{AS} = \beta - \xi_R(\beta - \kappa) \end{cases}$$

$$\text{if } \sigma < 0 \quad \begin{cases} \eta = -\varepsilon \\ R_s^{AS} = -\xi_S\beta + \xi_R(\beta - \kappa) \\ R_f^{AS} = -\beta + \xi_R(\beta - \kappa) \end{cases}$$

- Transition $S \to A$

$$\dot{\xi}_S^{SA} = -\pi^{SA}(\xi_S - \xi_R)\frac{\dot{G}^{SA}}{\left(S_f^{SA} - G^{SA}\right)^{\alpha^{SA}}}\mathscr{H}^{SA} \tag{10}$$

where

$$G^{SA} = \eta - \frac{C^{SA}}{E}T \tag{11}$$

$$S_f^{SA} = \frac{-C^{SA}T_f^{SA}}{E} + R_f^{SA} \tag{12}$$

$$S_s^{SA} = \frac{-C^{SA}T_s^{SA}}{E} + R_s^{SA} \tag{13}$$

with:

$$\text{if } \sigma \geqslant 0 \quad \begin{cases} \eta = \varepsilon \\ R_s^{SA} = \xi_S\beta - \xi_R(\beta - \kappa) \\ R_f^{SA} = \xi_R\kappa \end{cases}$$

$$\text{if } \sigma < 0 \quad \begin{cases} \eta = -\varepsilon \\ R_s^{SA} = -\xi_S\beta + \xi_R(\beta - \kappa) \\ R_f^{SA} = -\xi_R\kappa \end{cases}$$

The quantities C^{AS} and C^{SA} are the Clausius–Clapeyron constants for the phase transformations $A \to S$ and $S \to A$, respectively; they are set as $C^{AS} = C^{AS,+}$ and $C^{SA} = C^{SA,+}$ in tension and $C^{AS} = C^{AS,-}$ and $C^{SA} = C^{SA,-}$ in compression, as represented in Fig. 1; σ_s^{AS} and σ_f^{AS} are the starting and final stress for the $A \to S$ phase transformation at temperature $T = T_s^{AM}$; they are set as $\sigma_s^{AS} = \sigma_s^{AS,+}$ and $\sigma_f^{AS} = \sigma_f^{AS,+}$ in tension and $\sigma_s^{AS} = \sigma_s^{AS,-}$ and $\sigma_f^{AS} = \sigma_f^{AS,-}$ in compression, as represented in Fig. 1. The quantities π^{AS}, π^{SA}, α^{AS} and α^{SA} are material parameters.

Furthermore, $\mathscr{H}^{AS}$ and $\mathscr{H}^{SA}$ are activation factors, which are set as:

$$\mathscr{H}^{AS} = \begin{cases} 1 & \text{when} \quad \begin{cases} \dot{G}^{AS} > 0 \\ S_s^{AS} \leqslant G^{AS} \leqslant S_f^{AS} \end{cases} \\ 0 & \text{otherwise} \end{cases} \tag{14}$$

$$\mathscr{H}^{SA} = \begin{cases} 1 & \text{when} \quad \begin{cases} \dot{G}^{SA} < 0 \\ S_f^{SA} \leqslant G^{SA} \leqslant S_s^{SA} \end{cases} \\ 0 & \text{otherwise} \end{cases} \tag{15}$$

It can be pointed out that the phase transformations austenite–martensite and martensite–austenite cannot occur at the same time since when $\mathscr{H}^{AS} = 1$ then $\mathscr{H}^{SA} = 0$ and when $\mathscr{H}^{SA} = 1$ then $\mathscr{H}^{AS} = 0$. Thus only one of two evolutive equations (6) and (10) is not trivial and it has to be solved during the phase transformation.

The following evolutive equation is adopted for the parameter β that governs the reorientation process:

$$\dot{\beta} = \begin{cases} \gamma[\varepsilon_L \operatorname{sgn}(\sigma) - \beta][\operatorname{abs}(\sigma) - \sigma^{SS}] & \text{when } \operatorname{abs}(\sigma) > \sigma^{SS} \\ 0 & \text{otherwise} \end{cases} \tag{16}$$

where ε_L is a material constant measuring the maximum inelastic strain that is obtained by a complete conversion of austenite into martensite aligning all the single variant martensites in one direction, set as $\varepsilon_L = \varepsilon_L^+$ in tension and $\varepsilon_L = \varepsilon_L^-$ in compression, γ is a material parameter measuring the reorientation process rate and σ^{SS} is a limit stress which activates the reorientation process. It can be noted that σ^{SS} can assume different values in tension, $\sigma^{SS} = \sigma^{SS,+}$, and in compression, $\sigma^{SS} = \sigma^{SS,-}$. The training parameter κ is set as $\kappa = \varepsilon_L^+$ if the training is in tension and $\kappa = -\varepsilon_L^-$ if the training is in compression.

To properly simulate the training effects on the material, it is assumed that the initial and final stress thresholds of the phase transformations and the residual martensite fraction ξ_R depend on the loading history, as discussed in the following section.

2.3. Modelling of training effects

The characteristic behaviour of SMA under cyclic loading is illustrated in Fig. 2, where an experimental

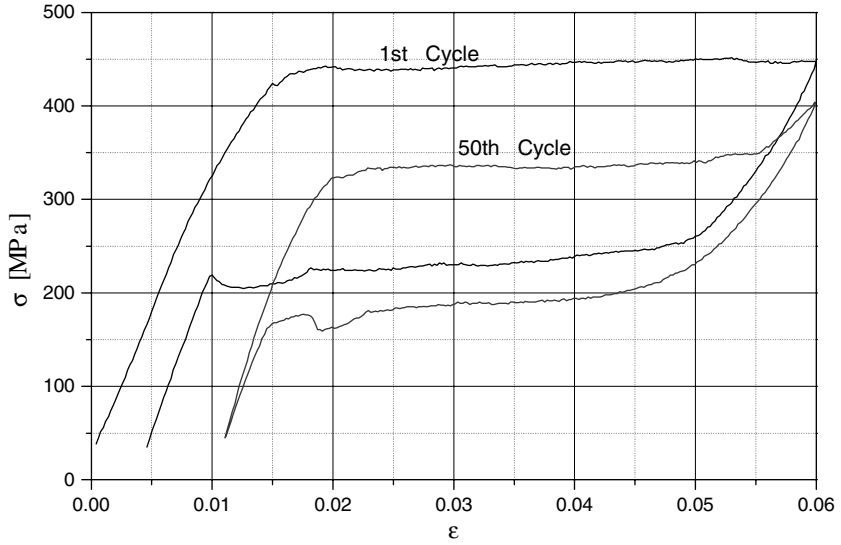

Fig. 2. Stress–strain response of a OMRCO wire of a circular section of Ni–Ti shape memory alloy under cyclic loading: experimental results.

test on a Ni–Ti wire of circular section, producted by OMRCO (Glendora, CA, USA), is described. The experimental stress–strain curve, reported in Fig. 2, represents the typical pseudoelastic mechanical response under cyclic loading of Ni–Ti shape memory alloy. This and several other tests on the same material were performed in the Laboratory of Biological Structure Mechanics (Labs) at the Politecnico of Milano (Italy). In Fig. 2, only the 1st and the 50th of the 100 performed cycles, are represented. The other cycles are not reported in order to obtain a more clear representation of the training effects. From the whole cyclic test, it results that in correspondence of the 50th cycle the material response has already reached a limit and stable path. It can be noted that the initial and final stress thresholds of the phase transformations austenite–martensite and martensite–austenite decrease during the cyclic loading of different quantities. Thus each value of the stress is bounded between two values. In particular, for the phase transformation $A \to S$ the values of σ_s^{AS} and σ_f^{AS} are limited between the following values:

$$\begin{aligned}&\text{For no-trained material (i.e. virgin)}\\ &\sigma_s^{AS} = \sigma_{s1}^{AS}\\ &\sigma_f^{AS} = \sigma_{f1}^{AS}\\ &\text{For fully-trained material}\\ &\sigma_s^{AS} = \sigma_{s2}^{AS}\\ &\sigma_f^{AS} = \sigma_{f2}^{AS}\end{aligned} \tag{17}$$

with $\sigma_{s1}^{AS} \geqslant \sigma_{s2}^{AS}$ and $\sigma_{f1}^{AS} \geqslant \sigma_{f2}^{AS}$.

In the phase transformation $S \to A$ the initial and final stress thresholds decrease as a consequence of the increase of the temperature T_s^{SA} and T_f^{SA} between two limit values denoted as:

$$\begin{aligned}&\text{For no-trained material (i.e. virgin)}\\ &T_s^{SA} = T_{s1}^{SA}\\ &T_f^{SA} = T_{f1}^{SA}\\ &\text{For fully-trained material}\\ &T_s^{SA} = T_{s2}^{SA}\\ &T_f^{SA} = T_{f2}^{SA}\end{aligned} \tag{18}$$

with $T_{s1}^{SA} \leqslant T_{s2}^{SA}$ and $T_{f1}^{SA} \leqslant T_{f2}^{SA}$.

Thus in the proposed model, it is assumed that σ_s^{AS}, σ_f^{AS}, T_s^{SA} and T_f^{SA} evolve between the two limiting values, reported in (17) and (18), following an exponential law in terms of accumulative measures of the phase transformation occurrence. In particular, it is set:

$$\sigma_s^{AS} = \sigma_{s1}^{AS} - (\sigma_{s1}^{AS} - \sigma_{s2}^{AS})[1 - \exp(-b_s^{AS}\gamma^{SA})] \tag{19}$$

$$\sigma_f^{AS} = \sigma_{f1}^{AS} - (\sigma_{f1}^{AS} - \sigma_{f2}^{AS})[1 - \exp(-b_f^{AS}\gamma^{SA})] \tag{20}$$

$$T_s^{SA} = T_{s1}^{SA} + (T_{s2}^{SA} - T_{s1}^{SA})[1 - \exp(-b_s^{SA}\gamma^{AS})] \tag{21}$$

$$T_f^{SA} = T_{f1}^{SA} + (T_{f2}^{SA} - T_{f1}^{SA})[1 - \exp(-b_s^{SA}\gamma^{AS})] \tag{22}$$

where

$$\dot{\gamma}^{AS} = \left|\dot{\xi}_S^{AS}\right| \qquad \dot{\gamma}^{SA} = \left|\dot{\xi}_S^{SA}\right| \tag{23}$$

and b_s^{AS}, b_f^{AS}, b_s^{SA} and b_s^{SA} are material constants measuring the material ability to be trained. The evolution

of the stress values σ_s^{AS} and σ_f^{AS} occurs during the $S \to A$ phase transformation, while the evolution of the temperature values T_s^{SA} and T_f^{SA} occurs during the $A \to S$ phase transformation. Eq. (19) is plotted in Fig. 3(a) for different values of b_s^{AS}. Similar curves can be derived for σ_f^{AS}, T_s^{SA} and T_f^{SA}.

Analogous considerations can be drawn for the residual martensite fraction ξ_R. In fact, from the experimental stress–strain curve reported in Fig. 2, it can be also pointed that the parameter ξ_R is bounded between two values; for no-trained material (i.e. virgin), it is $\xi_R = 0$, for fully-trained material, it is $\xi_R = \xi_L$.

Thus it is assumed that the residual martensite fraction ξ_R evolves between the two limiting values, 0 and ξ_L, following an exponential law in terms of an accumulative measure of the phase transformation occurrence. In particular, it is set:

$$\xi_R = \xi_L[1 - \exp(-b_R \gamma^{AS})] \tag{24}$$

where γ^{AS} is given by the first of the formulas (23) and b_R is a material constant measuring the material ability to be trained. The evolution of the residual martensite fraction ξ_R occurs during the $A \to S$ phase transforma-

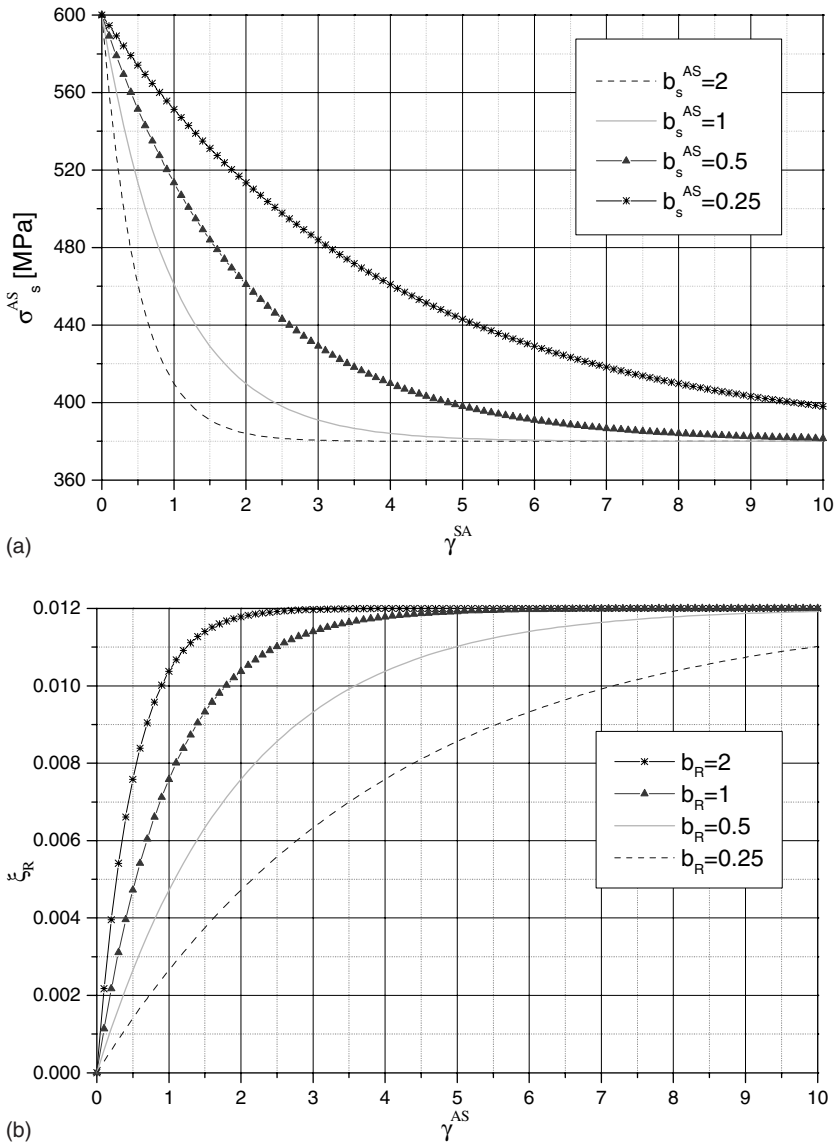

Fig. 3. Evolution σ_S^{AS} of as a function of γ^{SA} for different values of b_S^{AS} (a); evolution of ξ_R as a function of γ^{AS} for different values of b_R (b).

tion. Eq. (24) is plotted in Fig. 3(b) for different values of b_R.

3. Time-discrete model and solution algorithm

The evolutive equations governing the shape-memory alloys phase transformations are integrated developing a step by step time algorithm. In particular, once the solution at time t_n is known, a backward-Euler implicit integration procedure is adopted to evaluate the solution at time $t_{n+1} = t_n + \Delta t$. In the following the subscript 'n' indicates a quantity evaluated at the time t_n while no subscript indicates a quantity evaluated at the current time t_{n+1}. The symbol Δ indicates the variable increments at the time step Δt.

The discretization form of the evolutive equations (23) is:

$$\gamma^{AS} = \gamma_n^{AS} + (\xi_S^{AS} - \xi_{S,n}^{AS}) \qquad \gamma^{SA} = \gamma_n^{SA} - (\xi_S^{SA} - \xi_{S,n}^{SA}) \tag{25}$$

In Eq. (25) it is assumed that the conditions (14) and (15) for the phase transformation activation are satisfied. The time-discrete form of the evolutionary equations (6) and (10) written in a residual form is:

$$R_1 = \lambda_S^{AS}(S_{f,n}^{AS} - G^{AS})^{\alpha^{AS}} - \pi^{AS}(1 - \xi_S) \times (G^{AS} - G_n^{AS})\mathscr{H}^{AS} = 0 \tag{26}$$

$$R_2 = \lambda_S^{SA}(G^{SA} - S_{f,n}^{SA})^{\alpha^{SA}} - \pi^{SA}(\xi_S - \xi_R) \times (G^{SA} - G_n^{SA})\mathscr{H}^{SA} = 0 \tag{27}$$

where, the martensitic fraction variation is defined as:

$$\lambda_S^{AS} = \int_{t_n}^{t_{n+1}} \dot{\xi}_S^{AS}\,\mathrm{d}t \qquad \lambda_S^{SA} = \int_{t_n}^{t_{n+1}} \dot{\xi}_S^{SA}\,\mathrm{d}t \tag{28}$$

such that

$$\xi_S = \xi_{S,n} + \lambda_S^{AS} + \lambda_S^{SA} \tag{29}$$

Note that only one of two residual equations (26) and (27) is not trivial and it has to be solved during the phase transformation since, as it has been already pointed out, when $\mathscr{H}^{AS} = 1$ then $\mathscr{H}^{SA} = 0$ and when $\mathscr{H}^{SA} = 1$ then $\mathscr{H}^{AS} = 0$.

The two residual equations (26) and (27) are nonlinear so they are linearized by a Newton–Raphson technique. An iterative procedure is developed in order to evaluate λ_S^{AS} and λ_S^{SA} at each time step. In the following, the apex ^{k} denotes the quantities at the kth iteration and the apex $^{k+1}$ those at the current iteration. The symbol δ indicates the quantities variation between two consecutive iterations, i.e. $\delta\lambda_S = \lambda_S^{k+1} - \lambda_S^k$.

By linearization, Eqs. (26) and (27) become:

$$0 = R_1^{k+1} = R_1^k + \left.\frac{\mathrm{d}R_1}{\mathrm{d}\lambda_S^{AS}}\right|_k \delta\lambda_S^{AS} \tag{30}$$

$$0 = R_2^{k+1} = R_2^k + \left.\frac{\mathrm{d}R_2}{\mathrm{d}\lambda_S^{SA}}\right|_k \delta\lambda_S^{SA} \tag{31}$$

For $\mathscr{H}^{AS} = 1$, substituting formula (5), (7) and (29) in Eq. (26), it results:

$$R_1^k = \lambda_S^{AS,k}(L_1^{AS,k})^{\alpha^{AS}} - \pi^{AS}(1 - \xi_{S,n} - \lambda_S^{AS,k})L_2^{AS,k} \tag{32}$$

$$\left.\frac{\mathrm{d}R_1}{\mathrm{d}\lambda_S^{AS}}\right|_k = (L_1^{AS,k})^{\alpha^{AS}}\left(1 + \frac{\lambda_S^{AS,k}\alpha^{AS}C^{AS}T(E_A - E_S)}{E_A E_S L_1^{AS,k}}\right) + \pi^{AS}\left(L_2^{AS,k} + \frac{(1 - \xi_{S,n} - \lambda_S^{AS,k})C^{AS}T(E_A - E_S)}{E_A E_S}\right) \tag{33}$$

where

$$L_1^{AS,k} = S_{f,n}^{AS} - \eta + \frac{C^{AS}T(E_S + (\xi_{S,n} + \lambda_S^{AS,k})(E_A - E_S))}{E_A E_S} \tag{34}$$

$$L_2^{AS,k} = \eta - \frac{C^{AS}T(E_S + (\xi_{S,n} + \lambda_S^{AS,k})(E_A - E_S))}{E_A E_S} - G_n^{AS} \tag{35}$$

For $\mathscr{H}^{SA} = 1$, substituting formula (5), (11) and (29) in Eq. (27), it results:

$$R_2^k = \lambda_S^{SA,k}(L_1^{SA})^{\alpha^{SA}} - \pi^{SA}(\xi_{S,n} + \lambda_S^{SA,k} - \xi_R)L_2^{SA,k} \tag{36}$$

$$\left.\frac{\mathrm{d}R_2}{\mathrm{d}\lambda_S^{SA}}\right|_k = (L_1^{SA})^{\alpha^{SA}}\left(1 - \frac{\lambda_S^{SA,k}\alpha^{SA}C^{SA}T(E_A - E_S)}{E_A E_S L_1^{SA,k}}\right) - \pi^{AS}\left(L_2^{SA,k} + \frac{(\xi_{S,n} + \lambda_S^{SA,k} - \xi_R)C^{SA}T(E_A - E_S)}{E_A E_S}\right) \tag{37}$$

where

$$L_1^{SA,k} = \eta - \frac{C^{SA}T(E_S + (\xi_{S,n} + \lambda_S^{SA,k})(E_A - E_S))}{E_A E_S} - S_{f,n}^{SA}$$

$$L_2^{SA,k} = \eta - \frac{C^{SA}T(E_S + (\xi_{S,n} + \lambda_S^{SA,k})(E_A - E_S))}{E_A E_S} - G_n^{SA}$$

The single-variant martensite variation at each iteration results:

$$\delta\lambda_S^{AS} = -\left(\frac{dR_1}{d\lambda_S^{AS}}\bigg|_k\right)^{-1} R_1^k \qquad \delta\lambda_S^{SA} = -\left(\frac{dR_2}{d\lambda_S^{SA}}\bigg|_k\right)^{-1} R_2^k \tag{38}$$

so the variables λ_S^{AS} and λ_S^{SA} can be updated as:

$$\lambda_S^{AS,k+1} = \lambda_S^{AS,k} + \delta\lambda_S^{AS} \qquad \lambda_S^{SA,k+1} = \lambda_S^{SA,k} + \delta\lambda_S^{SA} \tag{39}$$

Then, the iterative procedure goes on until a convergence test is satisfied, i.e. when the values of the residuals computed by Eqs. (26) and (27) are less then a prefixed tolerance.

Setting the exponential $\alpha^{AS} = 1$ and $\alpha^{SA} = 1$ and the coefficients $\pi^{AS} = 1$ and $\pi^{SA} = 1$, Eqs. (26) and (27) become linear. In this case the evolution of ξ_S can be evaluated with explicit formula without using the Newton–Raphson technique, illustrated above, and it results:

$$\lambda_S^{AS} = \frac{(1-\xi_{S,n})\left(\eta - (E_S + \xi_{S,n}(E_A - E_S))\frac{C^{AS}}{E_A E_S}T - G_n^{AS}\right)}{(S_{f,n}^{AS} - G_n^{AS}) + (1-\xi_{S,n})(E_A - E_S)\frac{C^{AS}}{E_A E_S}T} \tag{40}$$

$$\lambda_S^{SA} = \frac{-(\xi_{S,n} - \xi_R)\left(\eta - (E_S + \xi_{S,n}(E_A - E_S))\frac{C^{SA}}{E_A E_S}T - G_n^{SA}\right)}{(S_{f,n}^{SA} - G_n^{SA}) - (\xi_{S,n} - \xi_R)(E_A - E_S)\frac{C^{SA}}{E_A E_S}T} \tag{41}$$

The time integration of the evolutive equation (16) of the reorientation parameter β when it occurs, i.e. when $\mathrm{abs}(\sigma) > \sigma^{SS}$, gives:

$$\beta = \beta_n + \begin{cases} \Delta t\ \gamma[\varepsilon_L - \beta][\sigma - \sigma^{SS}] & \text{when} \quad \sigma > \sigma^{SS} \\ \Delta t\ \gamma[\varepsilon_L + \beta][\sigma + \sigma^{SS}] & \text{when} \quad \sigma < -\sigma^{SS} \end{cases} \tag{42}$$

Then, parameter β is evaluated solving the second order equation obtained substituting the expression of σ, given by formula (4), into Eq. (42) [22].

The training equations do not contain rate terms, hence they are evaluated at time t_{n+1}:

$$\sigma_s^{AS} = \sigma_{s1}^{AS} - (\sigma_{s1}^{AS} - \sigma_{s2}^{AS})[1 - \exp(-b_\sigma \gamma^{SA})] \tag{43}$$

$$\sigma_f^{AS} = \sigma_{f1}^{AS} - (\sigma_{f1}^{AS} - \sigma_{f2}^{AS})[1 - \exp(-b_\sigma \gamma^{SA})] \tag{44}$$

$$T_s^{AS} = T_{s1}^{AS} + (T_{s2}^{AS} - T_{s1}^{AS})[1 - \exp(-b_\sigma \gamma^{AS})] \tag{45}$$

$$T_f^{AS} = T_{f1}^{AS} + (T_{f2}^{AS} - T_{f1}^{AS})[1 - \exp(-b_\sigma \gamma^{AS})] \tag{46}$$

$$\xi_R = \xi_L[1 - \exp(-b_R \gamma^{AS})] \tag{47}$$

It is interesting to note that within a generic time step $[t_n, t_{n+1}]$ the time-discrete model represents a nonlinear problem. Thus, a proper algorithm should be devised to compute the solution. Moreover, the specific algorithm should take into account a proper evaluation of the activation factors in a time-discrete setting.

3.1. Solution algorithm

The time-discrete model is solved adopting a return-map algorithm. Due to the fact that a phase transition phenomena is faced, the return map algorithm needs to be properly modified with respect to the one usually adopted for plasticity models.

Two trial states are defined for each phase transformation; the first trial state is obtained assuming no evolution for the phase transition and the second one is evaluated considering a complete transition evolution. If the first trial state violates the initial conditions for the phase transformation and the second trial state does not violate the final condition of the phase transformation a correction step is introduced. In the correction step, the Newton–Raphson technique, described in the previous section, is adopted to correct and to compute the exact solution and the values of all the variables, in particular the training parameters are updated.

The algorithm procedure for the two phase transformations is reported schematically in the following.

Solution scheme for the $A \to S$ phase transformation.

- Evaluate the phase transformation limit parameters:

$$S_{f,n}^{AS} = \frac{\sigma_f^{AS} - C^{AS}T_s^{AM}}{E_S} + R_{f,n}^{AS}$$

$$S_{s,n}^{AS} = \frac{\sigma_{s,n}^{AS} - C^{AS}T_s^{AM}}{E_n} + S_{s,n}^{AS}$$

$$S_{f,n}^{SA} = \frac{-C^{SA}T_f^{SA}}{E_n} + R_{f,n}^{SA}$$

$$S_{s,n}^{SA} = \frac{-C^{SA}T_s^{SA}}{E_n} + R_{s,n}^{SA}$$

- Compute trial states:
  First trial state: no phase transformation

$$\xi_s^{tr1} = \xi_{S,n}$$

$$E^{tr1} = \frac{E_A E_S}{E_S + \xi_S^{tr1}(E_A - E_S)}$$

$$G^{AS,tr1} = \eta - \frac{C^{AS}}{E^{tr1}}T$$

  Second trial state: full phase transformation

$$\xi_S^{tr2} = 1$$

$$E^{\mathrm{tr2}} = E_{\mathrm{S}}$$

$$G^{\mathrm{AS,tr2}} = \eta - \frac{C^{\mathrm{AS}}}{E^{\mathrm{tr2}}} T$$

- Check trial states:
  if $G^{\mathrm{AS,tr1}} < S^{\mathrm{AS}}_{\mathrm{s},n}$ then
    $\xi_{\mathrm{s}} = \xi_{\mathrm{s},n}$
    solution found
  else if $G^{\mathrm{AS,tr2}} > S^{\mathrm{AS}}_{\mathrm{f},n}$ then
    $\xi_{\mathrm{S}} = 1$
    solution found
  else
    solve $\mathrm{A} \to \mathrm{S}$ evolutionary equations:
    compute $\lambda^{\mathrm{AS}}_{\mathrm{S}}$ from the Newton–Raphson technique
    compute the training parameters $T^{\mathrm{SA}}_{\mathrm{s}}$, $T^{\mathrm{SA}}_{\mathrm{f}}$ and ξ_{R}
  endif

Solution scheme for the $S \to A$ phase transformation.

- Compute trial states:
  First trial state: no phase transformation

$$\xi^{\mathrm{tr1}}_{\mathrm{S}} = \xi_{\mathrm{S},n}$$

$$E^{\mathrm{tr1}} = \frac{E_{\mathrm{A}} E_{\mathrm{S}}}{E_{\mathrm{S}} + \xi^{\mathrm{tr1}}_{\mathrm{S}} (E_{\mathrm{A}} - E_{\mathrm{S}})}$$

$$G^{\mathrm{SA,tr1}} = \eta - \frac{C^{\mathrm{SA}}}{E^{\mathrm{tr1}}} T$$

  Second trial state: full phase transformation

$$\xi^{\mathrm{tr2}}_{\mathrm{S}} = \xi_{\mathrm{R}}$$

$$E^{\mathrm{tr2}} = \frac{E_{\mathrm{A}} E_{\mathrm{S}}}{E_{\mathrm{S}} + \xi^{\mathrm{tr2}}_{\mathrm{S}} (E_{\mathrm{A}} - E_{\mathrm{S}})}$$

$$G^{\mathrm{SA,tr2}} = \eta - \frac{C^{\mathrm{SA}}}{E^{\mathrm{tr2}}} T$$

- Check trial states:
  if $G^{\mathrm{SA,tr1}} > S^{\mathrm{SA}}_{\mathrm{s},n}$ then
    $\xi_{\mathrm{S}} = \xi_{\mathrm{S},n}$
    solution found
  else if $G^{\mathrm{SA,tr2}} < S^{\mathrm{SA}}_{\mathrm{f},n}$ then
    $\xi_{\mathrm{S}} = \xi_{\mathrm{R}}$
    solution found
  else
    solve $\mathrm{S} \to \mathrm{A}$ evolutionary equations:
    compute $\lambda^{\mathrm{SA}}_{\mathrm{S}}$ from the Newton–Raphson technique
    compute the training parameters $\sigma^{\mathrm{AS}}_{\mathrm{s}}$ and $\sigma^{\mathrm{AS}}_{\mathrm{f}}$
  endif

3.2. Algorithmic tangent modulus

In the following, the construction of the tangent modulus consistent with the time-discrete model is discussed.

The differentiation of the constitutive equation (4) gives:

$$\mathrm{d}\sigma = \left\{ E^* A[\varepsilon - \xi_{\mathrm{S}}\beta + \xi_{\mathrm{R}}(\beta - \kappa) - \alpha(T - T_0)] + E\left(1 - A\left(\beta - \frac{\partial \xi_{\mathrm{R}}}{\partial \xi_{\mathrm{S}}}(\beta - \kappa)\right) - B(\xi_{\mathrm{S}} - \xi_{\mathrm{R}})\right)\right\} \mathrm{d}\varepsilon \tag{48}$$

where

$$E^* = \frac{\partial E}{\partial \xi_{\mathrm{S}}} \qquad A = \frac{\partial \xi_{\mathrm{S}}}{\partial \varepsilon} = \frac{\partial \lambda^{\mathrm{AS}}_{\mathrm{S}}}{\partial \varepsilon} + \frac{\partial \lambda^{\mathrm{SA}}_{\mathrm{S}}}{\partial \varepsilon}$$
$$B = \frac{\partial \beta}{\partial \varepsilon} \qquad C = \frac{\partial \xi_{\mathrm{R}}}{\partial \xi_{\mathrm{S}}} = \mathscr{H}^{\mathrm{AS}} \xi_{\mathrm{L}} b_{\mathrm{R}} \exp(-b_{\mathrm{R}} \gamma^{\mathrm{AS}}) \tag{49}$$

In particular, it is:

$$E^* = \frac{\partial E}{\partial \xi_{\mathrm{S}}} = -E^2 \frac{E_{\mathrm{A}} - E_{\mathrm{S}}}{E_{\mathrm{A}} E_{\mathrm{S}}} \tag{50}$$

For $\mathscr{H}^{\mathrm{AS}} = 1$, it results:

$$A = \frac{\pi^{\mathrm{AS}}(1 - \xi_{\mathrm{S},n} - \lambda^{\mathrm{AS}}_{\mathrm{S}})(L^{\mathrm{AS}}_1 - L^{\mathrm{AS}}_2 \alpha^{\mathrm{AS}})\mathrm{sgn}(\varepsilon)}{(L^{\mathrm{AS}}_1)^{\alpha^{\mathrm{AS}}+1} + \pi^{\mathrm{AS}} L^{\mathrm{AS}}_2 L^{\mathrm{AS}}_1 - \pi^{\mathrm{AS}}(1 - \xi_{\mathrm{S},n} - \lambda^{\mathrm{AS}}_{\mathrm{S}}) \frac{C^{\mathrm{AS}}}{E^2} T E^* (L^{\mathrm{AS}}_1 + L^{\mathrm{AS}}_2 \alpha^{\mathrm{AS}})} \tag{51}$$

$$L^{\mathrm{AS}}_1 = S^{\mathrm{AS}}_{\mathrm{f},n} - \eta + \frac{C^{\mathrm{AS}} T (E_{\mathrm{S}} + (\xi_{\mathrm{S},n} + \lambda^{\mathrm{AS}}_{\mathrm{S}})(E_{\mathrm{A}} - E_{\mathrm{S}}))}{E_{\mathrm{A}} E_{\mathrm{S}}} \tag{52}$$

$$L^{\mathrm{AS}}_2 = \eta - \frac{C^{\mathrm{AS}} T (E_{\mathrm{S}} + (\xi_{\mathrm{S},n} + \lambda^{\mathrm{AS}}_{\mathrm{S}})(E_{\mathrm{A}} - E_{\mathrm{S}}))}{E_{\mathrm{A}} E_{\mathrm{S}}} - G^{\mathrm{AS}}_n \tag{53}$$

For $\mathscr{H}^{\mathrm{SA}} = 1$, it results:

$$A = \frac{\pi^{\mathrm{SA}}(\xi_{\mathrm{S},n} + \lambda^{\mathrm{SA}}_{\mathrm{S}} - \xi_{\mathrm{R}})(L^{\mathrm{SA}}_1 - L^{\mathrm{SA}}_2 \alpha^{\mathrm{SA}})\mathrm{sgn}(\varepsilon)}{(L^{\mathrm{SA}}_1)^{\alpha^{\mathrm{SA}}+1} - \pi^{\mathrm{SA}} L^{\mathrm{SA}}_2 L^{\mathrm{SA}}_1 - \pi^{\mathrm{SA}}(\xi_{\mathrm{S},n} + \lambda^{\mathrm{SA}}_{\mathrm{S}} - \xi_{\mathrm{R}}) \frac{C^{\mathrm{SA}}}{E^2} T E^* (L^{\mathrm{SA}}_1 - L^{\mathrm{SA}}_2 \alpha^{\mathrm{SA}})} \tag{54}$$

$$L_1^{SA} = \eta - \frac{C^{SA}T(E_S + (\xi_{S,n} + \lambda_S^{SA})(E_A - E_S))}{E_A E_S} - S_{f,n}^{SA} \tag{55}$$

$$L_2^{SA} = \eta - \frac{C^{SA}T(E_S + (\xi_{S,n} + \lambda_S^{SA})(E_A - E_S))}{E_A E_S} - G_n^{SA} \tag{56}$$

The quantity B results for $\sigma > \sigma^{SS}$:

$$B = \frac{E^* A[\varepsilon - \xi_S\beta + \xi_R(\beta - \kappa) - \alpha(T - T_0)] + E(1 + (C - A)\beta)}{\frac{1 + \Delta t_\gamma[\sigma - \sigma^{SS}]}{\Delta t_\gamma(\varepsilon_L - \beta)} + E(\xi_S - \xi_R)} \tag{57}$$

and for $\sigma \leqslant \sigma^{SS}$:

$$B = \frac{E^* A[\varepsilon - \xi_S\beta + \xi_R(\beta - \kappa) - \alpha(T - T_0)] + E(1 + (C - A)\beta)}{\frac{1 - \Delta t_\gamma[\sigma + \sigma^{SS}]}{\Delta t_\gamma(\varepsilon_L + \beta)} + E(\xi_S - \xi_R)} \tag{58}$$

4. Numerical results

Some numerical applications are developed to assess the ability of the model to simulate typical SMA pseudoelastic strain–stress responses under cyclic loading conditions.

4.1. Cyclic behaviour

The experimental data relative to a nickel–titanium alloy are considered since Ni–Ti shape-memory alloys are probably the most frequently used in commercial applications. In particular, the experimental data presented in Reference [13] are taken in consideration. The material is a commercial pseudoelastic Ni–Ti straight wire with circular cross-section of diameter 2.01 mm.

From the inspection of the experimental data the parameters characterizing the tensile behaviour of material M1 for the proposed SMA model are reported in Table 1. Note that the data related to the compressive behaviour are not reported as only the tensile behaviour is investigated in the following.

In particular, two cyclic loading histories are considered.

In Fig. 4(a) the experimental stress–strain response of the material subjected to loading cycles characterized by the same maximum elongation equal to 7.0% is reported. As it can be seen in Fig. 4(a), during each cycle not complete phase transformations A → S and S → A occur and during the training there is a significant decrease of the initial stress threshold σ_S^{AS} and a relevant increase of the residual martensite fraction ξ_R.

In Fig. 4(b) the pseudoelastic response obtained by the proposed model is represented. It can be pointed out

Table 1
Material data for the three different SMA adopted for the numerical investigations

Material M1			
$E_A = 70000$ MPa	$E_S = 10000$ MPa	$\varepsilon_L^+ = 0.08$	
$T_s^{AM} = 10$ °C	$T_f^{AM} = 5$ °C	$T_{s1}^{SA} = 30$ °C	$T_{f1}^{SA} = 31$ °C
		$T_{s2}^{SA} = 30$ °C	$T_{f2}^{SA} = 31$ °C
$\sigma_{s1}^{AS,+} = 600$ MPa	$\sigma_{s2}^{AS,+} = 380$ MPa	$\sigma_{f1}^{AS,+} = 700$ MPa	$\sigma^{SS,+} = 30$ MPa
		$\sigma_{f2}^{AS,+} = 700$ MPa	
$C^{AS,+} = 6$ MPa/°C	$C^{SA,+} = 8$ MPa/°C	$\alpha = 0.00002$ °C^{-1}	$\xi_L = 0.012$
$\alpha^{AS} = 1.1$	$\pi^{AS} = 1.0$	$\alpha^{SA} = 1.0$	$\pi^{SA} = 0.97$
$b_s^{AS} = b_f^{AS} = 0.8$	$b_s^{SA} = b_f^{SA} = 0.8$	$b_R = 0.6$	
Material M2			
$E_A = 33000$ MPa	$E_S = 18300$ MPa	$\varepsilon_L^+ = 0.05$	$\xi_L = 0.125$
$T_s^{AM} = 4$ °C	$T_f^{AM} = 3$ °C	$T_{s1}^{SA} = 8$ °C	$T_{s2}^{SA} = 11$ °C
$T_{f1}^{SA} = 10$ °C	$T_{f2}^{SA} = 14$ °C		
$\sigma_{s1}^{AS,+} = 200$ MPa	$\sigma_{s2}^{AS,+} = 90$ MPa	$\sigma_{f1}^{AS,+} = 200$ MPa	$\sigma_{f2}^{AS,+} = 140$ MPa
$C^{AS,+} = 12$ MPa/°C	$C^{SA,+} = 15$ MPa/°C	$\sigma^{SS,+} = 30$ MPa	$\alpha = 0.00002$ °C^{-1}
$\alpha^{AS} = 1.1$	$\pi^{AS} = 1.0$	$\alpha^{SA} = 1.0$	$\pi^{SA} = 0.97$
$b_s^{AS} = b_f^{AS} = 0.1$	$b_s^{SA} = b_f^{SA} = 0.1$	$b_R = 0.5$	
Material M3			
$E_A = 33000$ MPa	$E_S = 18300$ MPa	$\varepsilon_L^+ = 0.08$	$\xi_L = 0.3$
$T_s^{AM} = 10$ °C	$T_f^{AM} = 5$ °C	$T_{s1}^{SA} = 28$ °C	$T_{f1}^{SA} = 32$ °C
		$T_{s2}^{SA} = 28$ °C	$T_{f2}^{SA} = 32$ °C
$\sigma_{s1}^{AS,+} = 40$ MPa	$\sigma_{f1}^{AS,+} = 80$ MPa	$\sigma^{SS,+} = 30$ MPa	$\alpha = 0.00002$ °C^{-1}
$\sigma_{s2}^{AS,+} = 40$ MPa	$\sigma_{f2}^{AS,+} = 80$ MPa		
$C^{AS,+} = 6$ MPa/°C	$C^{SA,+} = 8$ MPa/°C	$\alpha^{AS} = \alpha^{SA} = 1.0$	$\pi^{AS} = \pi^{SA} = 1.0$
$b_s^{AS} = b_f^{AS} = 0.2$	$b_s^{SA} = b_f^{SA} = 0.2$	$b_R = 0.5$	$T = 60$ °C

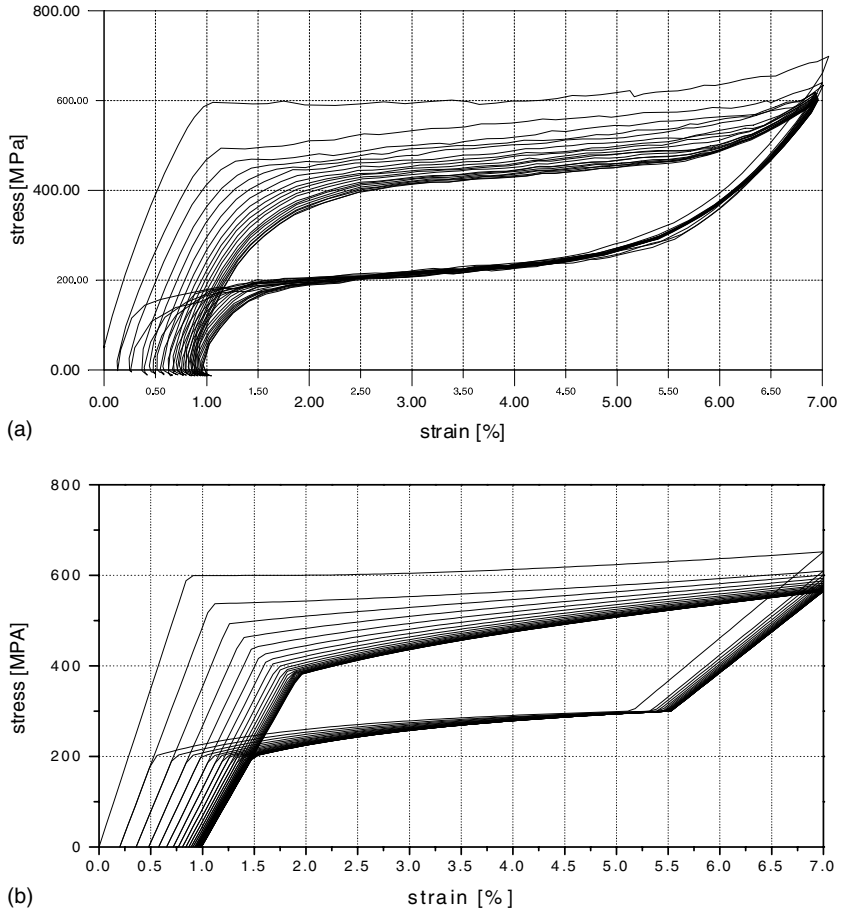

Fig. 4. Pseudoelastic response of a NiTi alloy subjected to equal loading cycles with 7% maximum elongation: experimental results (a); numerical results (b).

that the numerical response reported in Fig. 4(b) is in good accordance with the experimental behaviour reported in Fig. 4(a). The stress value σ_S^{AS} and the residual martensite fraction ξ_R vary more significantly in the first cycle then after 20 cycles the values of σ_S^{AS} and ξ_R tend to stabilize.

In Fig. 5(a) the evolution of the stress value σ_S^{AS} is plotted in terms of the accumulated strain during the $S \to A$ phase transformation, defined as $g^{SA} = \gamma^{SA}\varepsilon_L$, and in Fig. 5(b) the residual martensite fraction ξ_R versus the accumulated strain during the $A \to S$ phase transformation, set as $g^{AS} = \gamma^{AS}\varepsilon_L$, is represented. The experimental data and numerical results are represented with diamonds and with a continuous line, respectively. It can be noted that the experimental and numerical data are in a very good accordance, thus the choice of the model parameters is satisfactory. In particular, the model is able to simulate the evolution of the stress value σ_S^{AS} and of the residual martensite fraction ξ_R during the cyclic loading. Furthermore both the decrement of the stress threshold value σ_S^{AS} and the increment of the residual martensite fraction ξ_R tend to stabilize after the first 20 cycles.

In Fig. 6(a) the experimental stress–strain response of the material subjected to different loading cycles characterized by an increasing value of the maximum elongation that varies from 2% to 8% is plotted.

In Fig. 6(b) the mechanical pseudoelastic response obtained by the proposed model is represented. It can be pointed out that the numerical results (see Fig. 6(b)) are in good accordance with the experimental results (see Fig. 6(a)). In Fig. 7(a) the stress value σ_S^{AS} is plotted in terms of the accumulated strain g^{SA} and in Fig. 7(b) the residual martensite fraction ξ_R versus the accumulated strain g^{AS} is represented. It can be pointed out that the variation of σ_S^{AS} and of ξ_R, occurring during the $S \to A$ and the $A \to S$ phase transformations, respectively, are influenced by two opposite effects; the variations of the parameters σ_S^{AS} and ξ_R tend to decrease as these parameters are modelled adopting

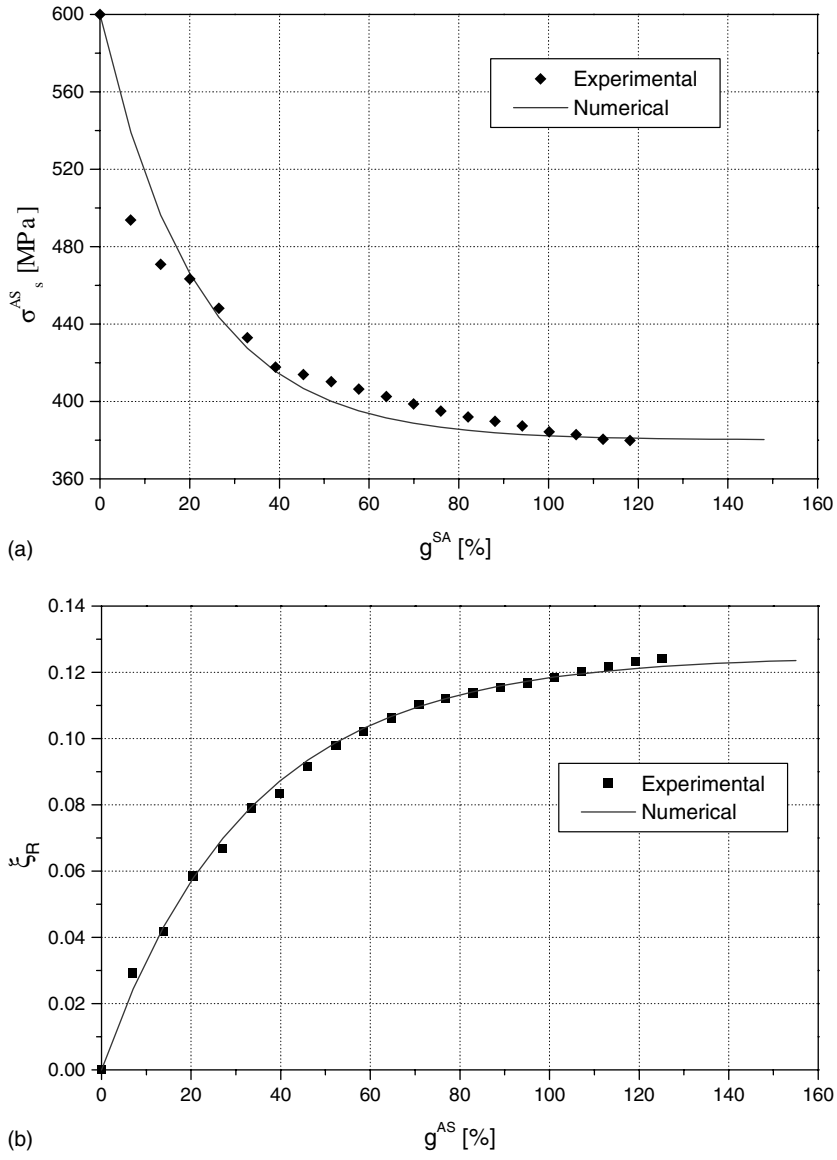

Fig. 5. Evolution of σ_S^{AS} as a function of the accumulated strain g^{SA} (a); evolution of ξ_R as a function of the accumulated strain g^{AS} (b).

exponential functions (19) and (24), on the other hand they tend to increase as a consequence of the increasing of the maximum deformation of the loading cycles.

Also in this case, the experimental and numerical data are in a very good accordance, thus the choice of the model parameters appears satisfactory.

Then, the experimental data related to the OMRCO wire of circular section of Ni–Ti shape memory alloy, represented in Fig. 2, are taken in consideration. The experimental stress–strain curve represents the pseudo-elastic mechanical response of the wire subjected to loading cycles characterized by the same maximum elongation equal to 6%. The parameters of the material M2 are set on the basis of the experimental data. In the following the tensile behaviour of the wire is investigated, thus only the parameters characterizing the tensile response are reported in Table 1.

In Fig. 8 the stress–strain response of the OMRCO wire is represented and in particular the 1st and the 50th cycle are plotted. It can be pointed out that experimental and numerical results are in a very good accordance. The proposed model is able to catch the variation of the initial and final stress thresholds of the phase transformations and the increment of permanent deformation.

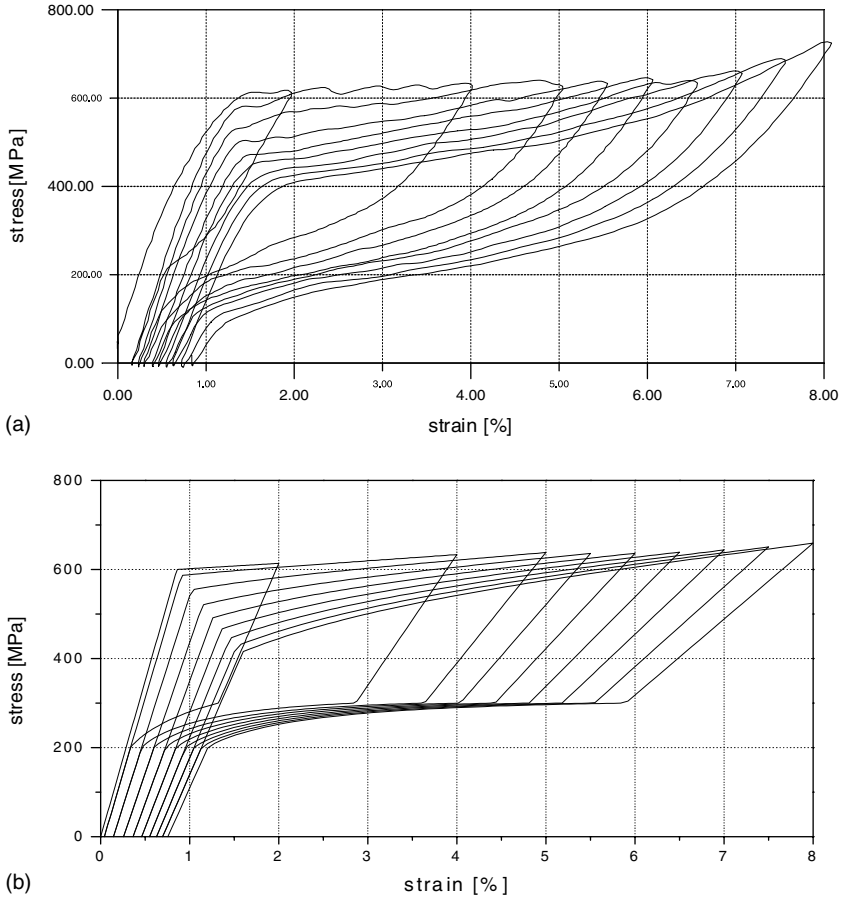

Fig. 6. Pseudoelastic response of a NiTi alloy subjected to loading cycles with an increasing maximum elongation from 2% to 8%: experimental results (a); numerical results (b).

4.2. Two way shape memory effect

A cantilever beam characterized by an elastic core and two SMA layers one on the top and the other on the bottom is analyzed. It is assumed that the shape memory alloy has the same mechanical behaviour in tension and in compression so only the data characterizing the tensile behaviour of material M3 are reported in Table 1.

Three analyses are performed using different values for the Young modulus of the elastic core:

1st case $E = 10000$ MPa
2nd case $E = 20000$ MPa
3rd case $E = 30000$ MPa

The beam length is equal to 10.0 mm, the rectangular cross section is 1.0 mm$\times$1.0 mm and each SMA layer has thickness equal to 0.1 mm so the elastic core thickness is of 0.8 mm.

The beam finite element developed in [22] is adopted to perform the numerical analyses.

In order to obtain a fully trained shape memory material the beam is subjected to a initial history of 10 cycles of bending loading–unloading, with a maximum bending moment equal to 200 Nmm at a constant temperature $T = 60$ °C. The whole training takes 20 s. In Fig. 9 the loading–unloading bending moment is plotted versus the transversal displacement of the free end of the beam for the three examined cases. It can be pointed out that after 10 cycles the mechanical response of the beam is stable in all the three cases as the SMA material is completely trained. Then, the beam is subjected to 2 cycles of change of temperature, ranging between 11 and 100 °C.

In Fig. 10 the transversal displacement of the beam free end is plotted versus time for the three different values of the elastic core Young modulus. It can be noted that at the end of the bending training, i.e. at the time $t = 20$ s, the beam remains in a deformed configuration because of the permanent strain accumulated during the cycles. After that time, i.e. for $t > 20$ s, two thermal cycles are performed, thus the beam swings

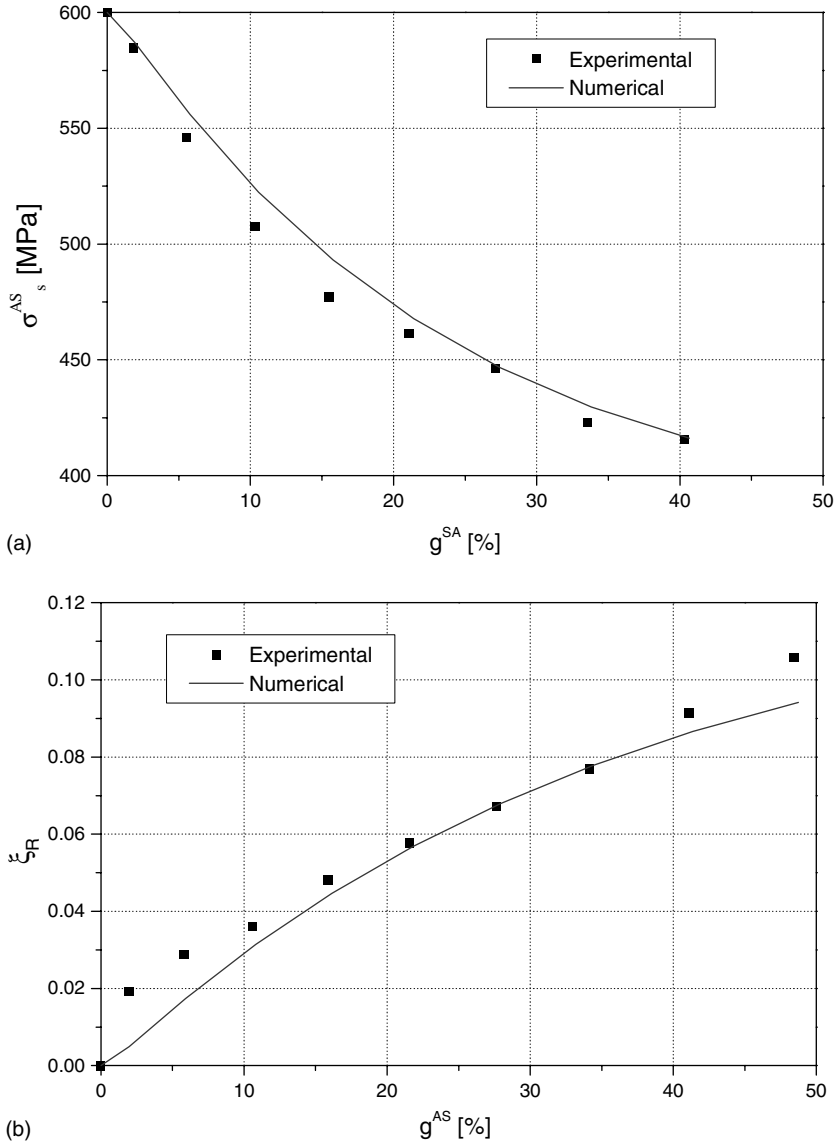

Fig. 7. Evolution of σ_S^{AS} as a function of the accumulated strain g^{SA} (a); evolution of ξ_R as a function of the accumulated strain g^{AS} (b).

between two configurations: the beam is able to recover a greater part of the permanent strain during cooling, while it goes back to the deformed shape during heating. Moreover the influence of the Young modulus of the elastic core on the described two way shape memory effect is small.

5. Conclusions

In the present work a one-dimensional (1D) model able to reproduce the pseudoelastic and the shape memory effect for shape-memory alloys under cyclic loading conditions is presented.

The model is based on scalar internal variables: the martensite fraction and the variables representing the material training effects. In particular, the training effects characterizing the pseudoelastic and shape memory behaviour under cyclic loading conditions, such as the variation of the initial and final stress thresholds of the phase transformations and of the residual martensite fraction, are modelled. The relatively large set of parameters is necessary for modelling such complex phenomena. Since the model parameters have a clear physical meaning they can be

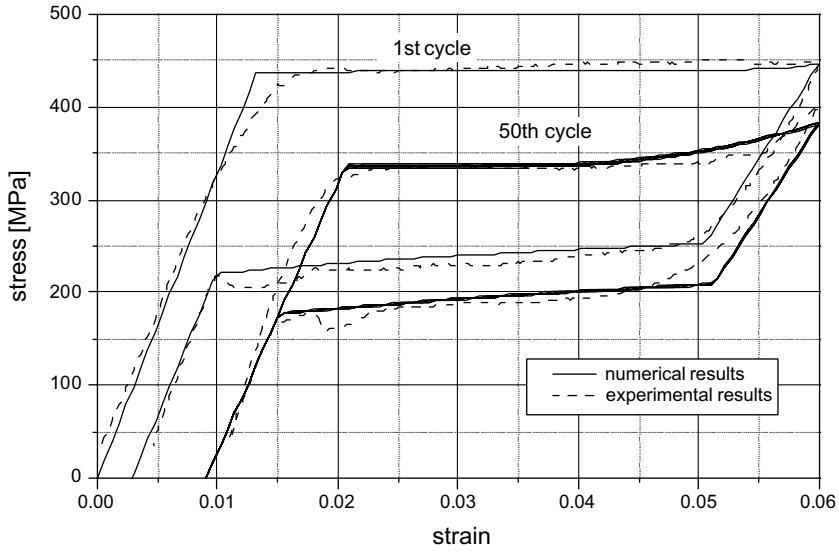

Fig. 8. Stress–strain response of a OMRCO wire under cyclic loading: comparison between experimental and numerical results.

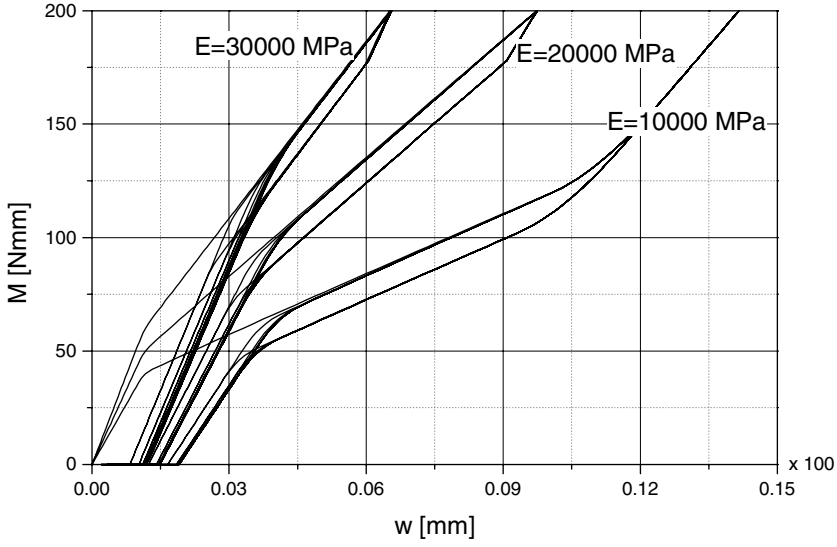

Fig. 9. Bending moment versus transversal displacement for three different values of the Young modulus of the elastic core.

set by performing suitable tensile and compressive experimental tests.

Attention is devoted to the integration of the model and to the formulation of a solution algorithm. The latter is obtained from a well-known family of elastic predictor–inelastic corrector algorithms, properly modified to take into account the type of evolution processes occurring in shape-memory materials. This aspect is of non-negligible interest for the development of computational tools to be used during the design process of SMA-based devices.

The capacity of the model to reproduce experimental data and the two way shape memory effect has also been assessed. Its ability to describe the material response for complex loading history (partial loading–unloading pattern) has been numerically tested.

The presented model results simple and able to properly reproduce the pseudoelastic and shape-memory

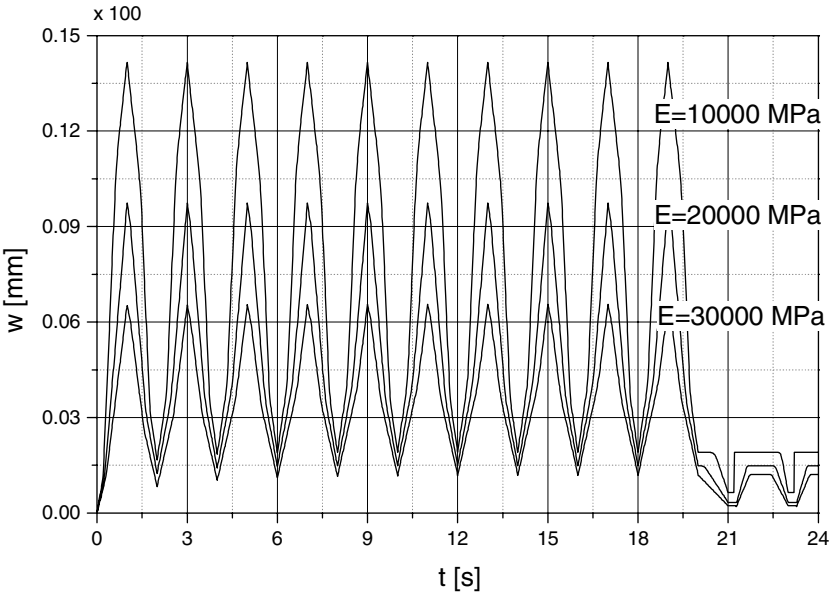

Fig. 10. Transversal displacement versus time for three different values of the Young modulus of the elastic core.

behaviour in tension and bending under cyclic loading conditions.

Acknowledgements

The present work has been partially developed within the joint French-Italian "Lagrangian laboratory" project as well as partially supported by the Italian National Center of Research (C.N.R.) and the University of Cassino.

References

[1] Abeyaratne R, Knowles J. On the driving traction acting on a surface of strain discontinuity in a continuum. J Mech Phys Solids 1990;38:345–60.
[2] Abeyaratne R, Sang-Joo Kim. Cyclic effects in shape memory alloys:a one-dimensional continuum model. Int J Solids Struct 1997;34:3273–89.
[3] Auricchio F. Shape memory alloys: applications, micromechanics, macromodelling and numerical simulations. PhD dissertation, University of California at Berkeley, Department of Civil Engineering, 1995.
[4] Auricchio F, Taylor RL, Lubliner J. Shape-memory alloys: macromodelling and numerical simulations of superelastic behavior. Comput Meth Appl Mech Eng 1997;146:281–312.
[5] Auricchio F, Sacco E. A 1D model for superelastic shape-memory alloys with different elastic properties between austenite and martensite. J Non-linear Mech 1997:1101–14.
[6] Auricchio F, Sacco E. A superelastic shape-memory alloy beam model. J Intel Mater Syst Struct 1997:1–13.
[7] Auricchio F, Sacco E. A temperature-dependent beam for shape-memory alloys: constitutive modelling, finite-element implementation and numerical simulations. Comput Meth Appl Mech Eng 1999;174:171–90.
[8] Auricchio F, Sacco E. Thermo-mechanical modelling of a superelastic shape-memory wire under cyclic stretching-bending loadings. Int J Solids Struct 2001;38:6123–45.
[9] Auricchio F, Faravelli L, Magonette G, Torra V, editors. Shape Memory Alloys. Advances in Modelling and Applications. CIMNE 2001, Barcelona.
[10] Zhonghe Bo, Lagoudas DC. Thermomechanical modeling of polycrystalline SMAs under cyclic loading, Part III: evolution of plastic strains and two-way shape memory effect. Int J Eng Sci 1999;37:1175–203.
[11] Boyd J, Lagoudas DC. A thermodynamical constitutive model for shape-memory materials. Part I. The monolithic shape-memory alloy. Int J Plast 1996;12:805–42.
[12] Buehler WJ, Wiley RC. Nickel-based alloys. Technical Report, 1965. US-Patent 3174851.
[13] Castellano MG, editor. Proceeding of the Final Workshop of ISTECH Project: Shape Memory Alloy Devices for Seismic Protection of cultural heritage Structures. June 23, 2000, Ispra, Italy.
[14] Duerig TW, Melton KN, Stökel D, Wayman CM, editors. Engineering aspects of shape-memory alloys. Butterworth-Heinemann; 1990.
[15] Falk F. Pseudo-elastic stress–strain curves of polycrystalline shape memory alloys calculated from single crystal data. Int J Eng Sci 1989;27:277–84.
[16] Filip P, Mazanec K. The two way memory effect in TiNi Alloys. Scripta Mater 1996;35:349–54.
[17] Huang M, Brinson L. A multivariant model for single crystal shape memory alloy behavior. J Mech Phys Solids 1998;46:1379–409.

[18] Leclercq S, Lexcellent C. A general macroscopic description of the thermomechanical behavior of shape memory alloys. J Mech Phys Solids 1996;44:953–80.
[19] Lexcellent C, Goo B, Sun Q, Bernardini J. Characterization, thermomechanical behavior and micro-mechanical-based constitutive model of shape memory Cu–Zn–Al single crystal. Acta Materialia 1996;44:3772–80.
[20] Lexcellent C, Bourbon G. Thermodynamical model of cyclic behavior of Ti–Ni and Cu–Zn–Al shape memory alloys under isothermal undulated tensile tests. Mech Mater 1996;24:59–73.
[21] Lexcellent C, Leclercq S, Gabry B, Bourbon G. The two way shape memory effect of shape memory alloys: an experimental study and phenomenological model. Int J Plast 2000;16:1155–68.
[22] Marfia S, Reddy JN, Sacco E. Superelastic and shape memory effects for laminated beams. AIAA Journal, accepted for publication.
[23] Pelton AR, Hodgson D, Duerig T, editors. Proceedings of the First International Conference on Shape Memory and Superelastic Technologies, 1994.
[24] Raniecki B, Lexcellent C. Thermodynamics of isotropic pseudoelasticity in shape-memory alloys. Eur J Mech A: Solids 1998;17:185–205.
[25] Qidwai MA, Lagoudas DC. On thermomechanics and transformation surfaces of polycrystalline NiTi shape memory alloy material. Int J Plast 2000;16:1309–43.
[26] Siderey N, Patoor E, Berveiller M, Eberhardt A. Constitutive equations for polycrystalline thermoelastic shape memory alloys. Part I. Intergranular interactions and behavior of grains. Int J Solids Struct 1999;36:4289–315.
[27] Souza A, Mamiya E, Zouain N. Three-dimensional model for solids undergoing stress-induced phase transformations. Eur J Mech A: Solids 1998;17:789–806.
[28] Tanaka K, Nishimura F, Hayashi T, Tobushi H, Lexcellent C. Phenomenological analysis on subloops and cyclic behavior in shape memory alloy under mechanical. Mech Mater 1995;19:281–92.
[29] Wayman CM. Introduction to the crystallography of martensitic transformations. MacMillan; 1964.